Received: 1 February 2021 | Revised: 8 July 2021 | Accepted: 22 September 2021

IET Generation, Transmission & Distribution

DOI: 10.1049/gtd2.12321

The Institution of Engineering and Technology WILEY

ORIGINAL RESEARCH PAPER

Comparisons of transformer thermal behaviours between conventional disc type and S disc type windings

Xiang Zhang[1] | Qiang Liu[1] | Zhongdong Wang[1,2] | Mark Wilkinson[3]

[1] Department of Electrical and Electronic Engineering, The University of Manchester, Manchester, UK

[2] College of Engineering, Mathematics and Physical Sciences, University of Exeter, Exeter, UK

[3] Royal SMIT Transformers BV, Postbus 9107, 6500 HJ, Nijmegen, Netherlands

Correspondence
Zhongdong Wang,Department of Electrical and Electronic Engineering, The University of Manchester, Manchester M13-9PL, UK
Email: Zhongdong.Wang@manchester.ac.uk

Abstract

Controlling the highest temperature in the windings is the primary objective of transformer thermal design to guarantee designed transformer thermal life expectancy. Temperature rise test results of a transformer with computational fluid dynamics (CFD) modelling results are compared here to determine typical OD and ON flow rates in the transformer. It then presents CFD studies that compare the thermal behaviour of two types of disc-type windings. The S disc-type winding refers to one that has only axial cooling ducts and physically resembles a layer-type winding. The other type is of conventional disc-type winding. The S disc-type winding shows robust thermal performance due to its quasi-uniform flow distributions in the axial cooling ducts, irrespective of the total oil flow rates or the cooling modes. In contrast, the conventional disc-type windings converted from the S disc-type winding experience uneven flow distributions in the radial cooling ducts that can cause localised overheating. Control of oil flow distribution in conventional disc-type windings is found critical for its thermal design. Heat transfer for the S disc-type winding is further enhanced by axially partitioning the winding into multiple sections, which is optimized based on theoretical analyses and is then verified by CFD modelling.

1 | INTRODUCTION

The primary objective of transformer thermal design is to control the highest temperature in the winding, usually referred to as the hotspot temperature, in steady state under the limitations specified in international standards [1–3]. This is because the hotspot temperature causes the severest thermal ageing of the paper insulation and therefore determines the life expectancy of a transformer. In addition, high temperature or high rate of change of temperature can cause bubble formation in the oil-paper insulation system and therefore compromise its dielectric strength [1, 4, 5].

The cooling of the transformer winding is usually achieved by circulation of dielectric liquid, usually mineral oil, between the winding and the cooler/radiator. The circulation can be pump-driven or thermosiphon-driven, and a transformer can have multiple cooling modes with the pump on or off depending on the load condition [6].

The winding cooling performance depends on the winding geometry, the oil flow distribution in the winding and the oil properties. This paper focuses on the influence of winding geometry on the cooling performance.

Disc type windings are widely used in power transformers, where successive winding conductors/turns are radially arranged to form winding discs. Conventional disc-type windings possess radial cooling ducts formed by the presence of pressboard spacers between adjacent discs in an angularly periodic fashion. There are usually two sets of axial cooling ducts on the inner side and the outer side of the winding discs, formed by placing sticks between the winding and the pressboard cylinders, fitted in with the radial spacers. In addition, blocking washers are usually placed between certain discs to partition the winding into passes, and they block one of the axial cooling ducts alternately to form zigzag oil flow pattern among the winding passes.

For conventional disc-type windings, the influence of winding geometry on oil flow distribution are widely investigated. Fairly uniform oil flow distribution in the winding pass is preferred to avoid localized overheating. Flow distributions in pump-driven oil directed (OD) cooling modes are quite different from those of thermosiphon-driven oil nature (ON) cooling modes [7]. OD flow distributions feature higher flow rates in the top part of the pass and lower flow rates in the bottom part of the pass [7–10], whereas ON flow distributions demonstrate the opposite trend [11–14]. The pitfall of conventional disc-type winding thermal design for OD cooling modes is pumping the oil too hard or having a winding geometry with too high ratio of radial duct height to axial duct width and therefore causing severely uneven flow distribution or even reverse flows at the bottom of the pass [8, 10]. For ON cooling modes, severely uneven flow distributions or even reverse flows at the top part of the pass occur when the total oil flow rate in the winding is relatively low corresponding to the winding power losses [11, 12, 14, 15]. In addition, the number of discs per pass is also found influential [16].

To change the oil flow pattern, disc-type windings can also be arranged to provide extra axial cooling ducts within the winding by placing spacers between the successive radial turns [17]. To maintain a high space factor (the ratio of copper volume to total winding volume), turns are located directly onto each other in the axial direction, eliminating the radial cooling ducts [17]. These disc-type windings with only axial cooling ducts are commonly adopted by SGB-SMIT Group and are hereinafter referred to as S disc-type windings. S disc-type windings have the same electrical connection as conventional ones, but from a thermal perspective they resemble layer-type windings. The major difference between S disc-type windings and layer-type windings is that layer-type windings are electrically connected in the axial direction with uneven layer length and graded insulation arrangement [6]. S disc-type windings have even "layer" length and similar insulation arrangement as conventional disc-type windings. The thermal features of S disc-type windings will be applicable to layer-type windings.

This paper presents the thermal behaviour comparisons between conventional disc-type windings and S disc-type windings. The pros and cons of the winding geometries on cooling performance are identified, and heat transfer enhancement strategies for S disc-type windings or layer-type windings are provided. The winding geometry of the S disc-type winding under investigation is presented in Section 2, followed by Computational Fluid Dynamics (CFD) simulations and comparisons with factory temperature-rise tests results in Section 3. The S disc-type winding is then converted to conventional disc-type windings maintaining the same number of winding turns and overall winding dimensions in Section 4. The thermal behaviour comparisons between the S disc-type winding and conventional disc-type windings are shown in Section 5. Heat transfer enhancement for the S disc-type winding is presented in Section 6, followed by conclusion in Section 7.

2 | S DISC-TYPE WINDING UNDER INVESTIGATION

The S disc-type winding under investigation is a typical 400 kV rated HV winding. It has nine "layers" and ten axial cooling ducts with each axial duct width being 5 mm, as shown in Figure 1. The winding inner radius is 871 mm. Each winding turn is made of paper wrapped continuously transposed conductors (CTCs). The CTC conductors are simplified to be copper blocks wrapped with 0.59 mm thick paper and the CTC overall radial width being 17.17 mm and axial height of 9.41 mm. There are 184 CTC conductors in each winding "layer" from bottom to top. There is an opening in the middle of the stress/shield ring with a width of 20 mm and this opening is

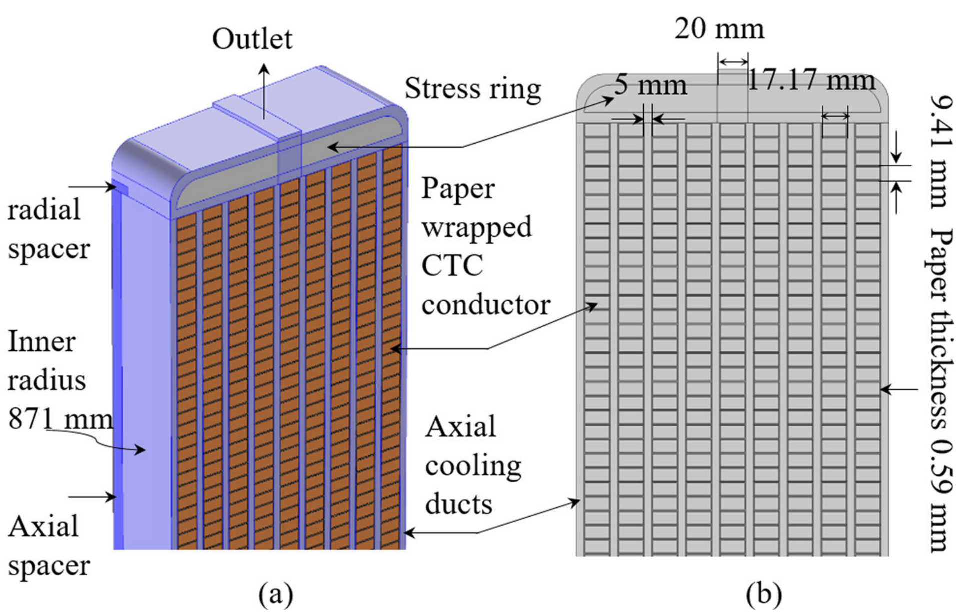

FIGURE 1 Geometry of the S disc-type winding under investigation. (a) 3D geometry. (b) 2D slice with geometric dimensions denoted

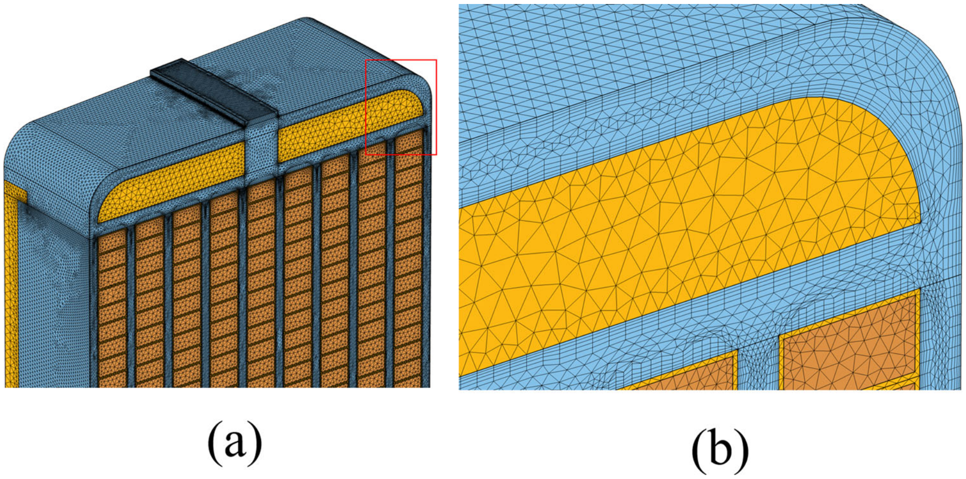

FIGURE 2 S disc-type winding mesh. (a) Mesh of the top part of the S disc-type winding. (b) Close-up of the top right corner in the red box

the outlet to the oil ducts created by angle rings. The top and bottom winding structures are identical, and the winding has an angular periodicity, so only a sectional view of the repeating top winding structure is shown in Figure 1.

3 | NUMERICAL SIMULATION AND COMPARISONS WITH TEMPERATURE RISE TESTS

3D CFD simulations of the HV winding in temperature-rise tests in steady states were conducted using COMSOL Multiphysics 5.4. Laminar flow and compressible liquid conditions were assumed in the CFD models. The validity of the CFD modelling tool and methods the authors adopted is proven by flow and temperature measurements of experiment test setups in the authors' previous publications [10, 14, 18]. The temperature deviations between CFD simulations and experimental test results were within 3 °C [10] with closely matched flow distributions [10, 14, 18]. Mesh refinement studies were conducted to guarantee mesh independent solutions. The mesh of the top part of the S disc-type winding is shown in Figure 2. Tetrahedrons were used to resolve the solid domains and the bulk oil domain. Five layers of flat cuboids were used to resolve the fluid boundaries and capture the hydraulic and thermal boundary layers. In total, 35,138,222 elements were created for the S disc-type winding.

The power losses in the CFD simulations were based on electromagnetic calculations from the transformer design stage, considering both resistive losses and eddy current losses. Here, nonuniform power losses of the S disc-type winding were provided by the manufacturer. The nonuniform power losses are symmetric in the axial direction. Therefore, only the power loss distribution in the bottom 20 discs is shown in Figure 3, which mirrors the loss distribution in the top 20 discs. The middle discs of the winding are set to have identical power losses of 160 W/conductor. Since the exact total oil flow rate in the HV winding is unknown, CFD sweeps of the oil flow rates were conducted for both OD and ON cooling modes. To determine the total oil flow rate, the average winding temperatures from CFD simulations were compared with corresponding temperature-rise test results. The top oil temperature comparison was not taken as the criterion because the top oil temperatures from the CFD simulations are from the outlet of the HV winding, while the top oil temperatures from temperature-rise tests are from the oil pocket at the top of the tank where oil from different paths including cold by-pass oil merge. IEC 60076–7 (2018) states that "measurements have shown that the top-oil temperature inside a winding might be, dependent on the cooling, up to 15 K higher than the mixed top-oil temperature inside the tank" [1].

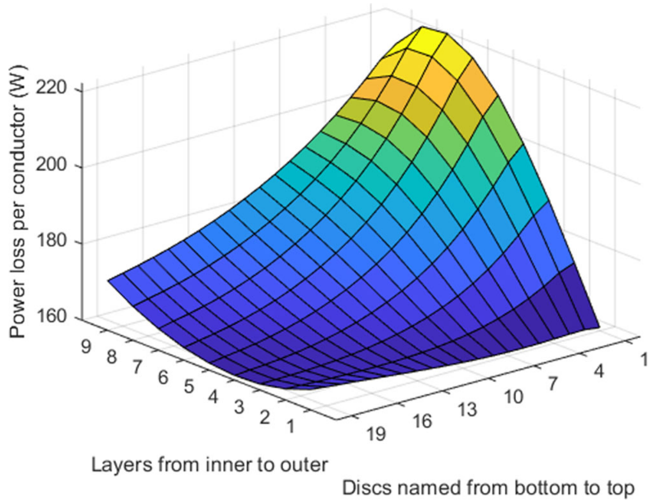

FIGURE 3 Nonuniform power loss at the bottom 20 discs of the winding

3.1 | OD cooling mode

In the OD temperature-rise test, the ambient temperature was 25.5 °C, and bottom oil temperature was 59.0 °C, which with a

TABLE 1 Sweep of HV winding inlet velocity with non-uniform power losses for the OD cooling mode (Ambient temperature 25.5 °C)

	Bottom oil (°C)	Top oil (°C)	Average winding (°C)	Hotspot (°C)	Hotspot factor
Temperature rise test	59.0 (33.5 K)	67.5 (42 K)	86.5 (61 K)	–	–
0.16 m/s	59.0	66.8	79.8	89.6	1.35
0.14 m/s	59.0	67.9	80.8	91.1	1.34
0.12 m/s	59.0	69.5	81.9	93.0	1.33
0.1 m/s	59.0	71.8	83.4	95.5	1.32
0.09 m/s	59.0	73.4	84.3	97.1	1.31
0.08 m/s	59.0	75.4	85.5	99.0	1.29
0.07 m/s	59.0	78.0 (52.5 K)	86.8 (61.3 K)	101.4 (75.9 K)	1.28
0.06 m/s	59.0	81.5	88.5	104.4	1.25
0.05 m/s	59.0	86.2	90.8	108.6	1.23

TABLE 2 Sweep of HV winding inlet velocity with non-uniform power losses for the ON cooling mode (Ambient temperature 27.7 °C)

	Bottom oil (°C)	Top oil (°C)	Average winding (°C)	Hotspot (°C)	Hotspot factor
Temperature rise test	40.0 (12.3 K)	63.7 (36 K)	62.5 (34.8 K)	–	–
0.03 m/s	40.0	51.3	51.0	58.4	1.33
0.02 m/s	40.0	57.3	53.9	64.0	1.28
0.016 m/s	40.0	61.8	56.1	68.2	1.23
0.012 m/s	40.0	69.2	59.7	75.0	1.14
0.011 m/s	40.0	71.8	61.0	77.5	1.12
0.01 m/s	40.0	74.9 (47.2 K)	62.5 (34.8 K)	80.4 (52.7 K)	1.09
0.009 m/s	40.0	78.6	64.4	84.0	1.06
0.008 m/s	40.0	82.7	66.4	87.9	1.03

uniform profile was used as the winding inlet temperature in the CFD sweep. The swept winding inlet velocities range from 0.05 to 0.16 m/s. All the winding inlet velocities are treated as fully developed, that is, with parabolic velocity profiles. The winding inlet velocity and temperature profiles represent the cooling effect of the cooler and tank. The case with inlet velocity being 0.07 m/s is a close match of the average winding temperature rise over the ambient temperature to the temperature-rise test result. The top oil temperature rise is 52.5 K, which is 10.5 K higher than the measured top oil temperature rise in the oil pocket, which agrees with the statement about top oil temperature difference between top of the winding and top of the tank from IEC 60076–7 (2018). The CFD top oil temperature rise is still lower than the 60 K top oil temperature rise limit stated in IEC 60076-2. The hotspot temperature rise is 75.9 K, lower than the 78 K limit in the same standard. The CFD sweep showed that the top oil, average winding and hotspot temperatures decrease with the increase in total oil flow rate in the winding, while the hotspot factor has the opposite trend, as shown in Table 1. It indicates that the lower the total oil flow rate the more linear the winding temperature distribution in the axial direction.

3.2 | ON cooling mode

In the ON temperature-rise test, the ambient temperature was 27.7 °C, and bottom oil temperature was 40.0 °C. In the ON CFD sweep, the power losses were set to be a quarter of the OD losses because of half of the rated load under the ON cooling mode. The swept winding inlet velocities range from 0.008 to 0.03 m/s. The case with inlet velocity being 0.01 m/s is a match of the average winding temperature rise over the ambient temperature. In the ON cooling mode, the top oil, average winding and hotspot temperature rises are much lower than the limits set in international standards. It is worth noting that the average winding temperature is lower than the top oil temperature and the hotspot factor decreases with the decrease in total oil flow rate, as shown in Table 2.

4 | CONVERSION TO CONVENTIONAL DISC-TYPE WINDING

To compare the thermal behaviour of the S disc-type winding with conventional disc-type windings in a fair manner, the

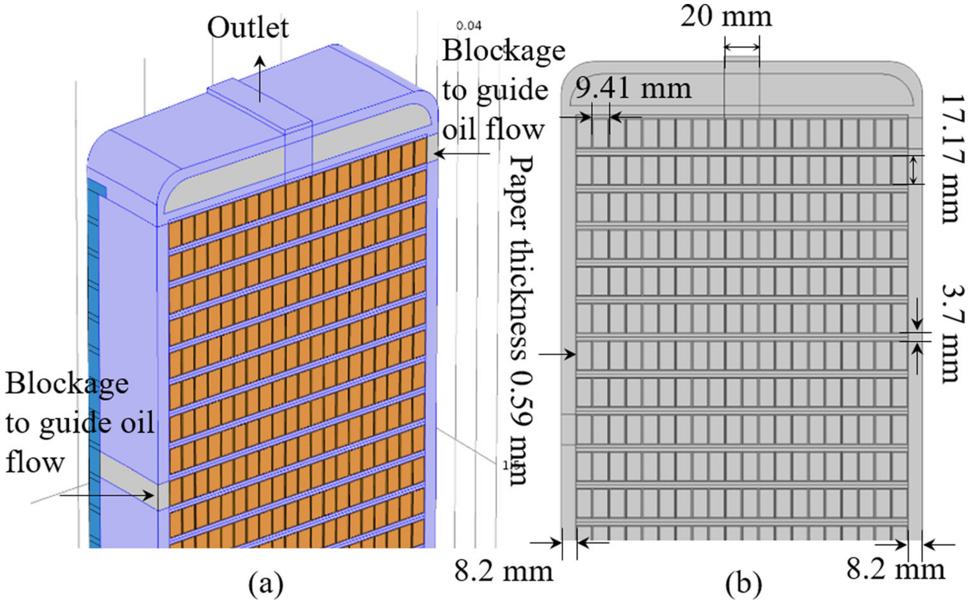

FIGURE 4 Converted conventional disc-type winding. (a) 3D geometry, (b) 2D slice with geometric dimensions denoted

S disc-type winding is converted to conventional disc-type windings with the same winding overall dimensions, identical conductor sizes and similar number of total conductors, as shown in Figure 4. In the converted conventional disc-type winding, the conductors are rotated 90 degrees. There are 83 discs with 20 conductors per disc and therefore 1660 conductors in total, which is close to the 1656 conductors in the original S disc-type winding. The horizontal duct height is 3.7 mm and vertical duct width of 8.2 mm to keep an identical space factor as the original one. Blockages are added next to discs to partition the winding into passes. Five-pass and ten-pass conventional disc-type windings were created with the top and bottom winding structures kept unchanged, as shown in Figure 4.

5 | THERMAL BEHAVIOUR COMPARISONS

In the comparisons, the power loss in the conductor is set to be uniform, corresponding only to the resistive power losses of 160 W/conductor to ensure that the only controlling parameter in the comparisons is geometry. The power loss in the ON cooling mode is a quarter of that of the OD cooling mode.

5.1 | OD cooling modes

For CFD comparisons in the OD cooling mode, the winding inlet velocity is 0.07 m/s. The flow distribution in the axial cooling ducts of the S disc-type winding is shown in Figure 5a, and the flow distributions for the 5-pass and 10-pass conventional disc-type windings are shown in Figure 5b. The flow distribution in the axial ducts of the S disc-type winding is quasi-uniform with lower flow rates in the inner and outer most two axial ducts, where the ducts are one-side heated. The flow distributions in the radial ducts of conventional disc-type winding are uneven. The 10-pass winding shows a clear trend of higher flow rates in the pass top ducts and lower rates in the bottom ducts. The 5-pass winding has the lowest flow rates in the middle radial ducts and a similar overall flow distribution trend as the 10-pass winding.

The temperature distributions correspond to the flow distributions. For the S disc-type winding, the temperature distribution in the radial direction is quasi-uniform, as shown by the temperature contour in Figure 6a, because of the uniform power loss and quasi-uniform flow distribution in the axial cooling ducts. The variation of the maximum conductor temperature in the radial direction with the conductor axial position from bottom to top is shown in Figure 7a. The drop of the conductor temperatures at the top of the S disc-type winding is caused by the radial cooling duct between the winding and the stress ring. The variations of the disc maximum temperatures of the 5-pass and 10-pass conventional disc-type windings with the disc position from bottom to top are shown in Figure 7b. The highest temperature in the pass corresponds to the lowest flow rate in the pass. The rise of the top disc temperature in each pass is because the top disc is adjacent to the bottom radial duct of the downstream pass, where the oil flow rate is relatively low. The temperature contours of the 5-pass and 10-pass windings are shown in Figures 6b and 6c, respectively.

With the same winding total oil flow rate, S disc-type winding has higher average winding and hotspot temperatures but with a much lower pressure drop over the winding, as shown in Table 3. It is worth noting that the 5-pass winding and the 10-pass winding have similar average winding temperatures and identical hotspot temperatures, indicating that it is not necessarily better to partition the winding into more passes and control of flow distribution is essential.

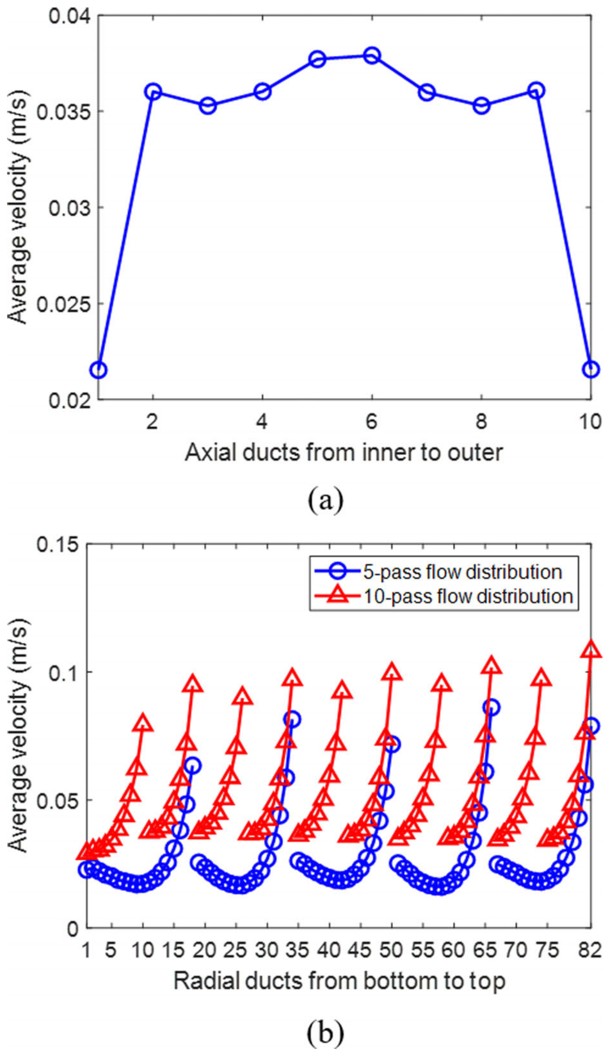

FIGURE 5 Flow distributions in the OD cooling mode with winding inlet velocity being 0.07 m/s. (a) Flow distribution in S disc-type winding axial ducts. (b) Flow distribution in 5-pass and 10-pass disc-type winding radial ducts

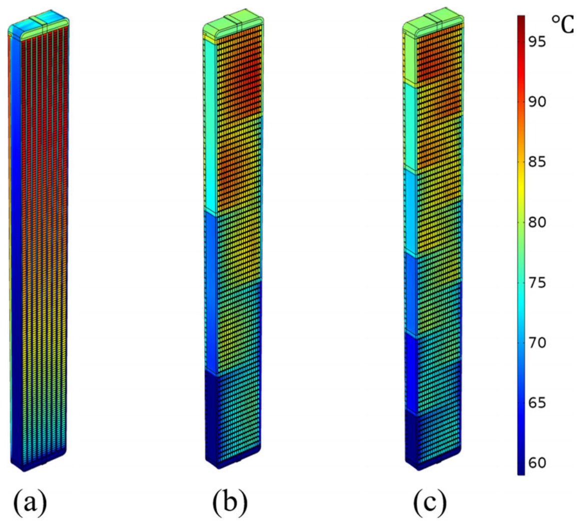

FIGURE 6 Temperature contours for the OD cooling mode with uniform OD power loss and winding inlet velocity 0.07 m/s. (a) S disc-type winding. (b) 5-pass disc-type winding. (c) 10-pass disc-type winding

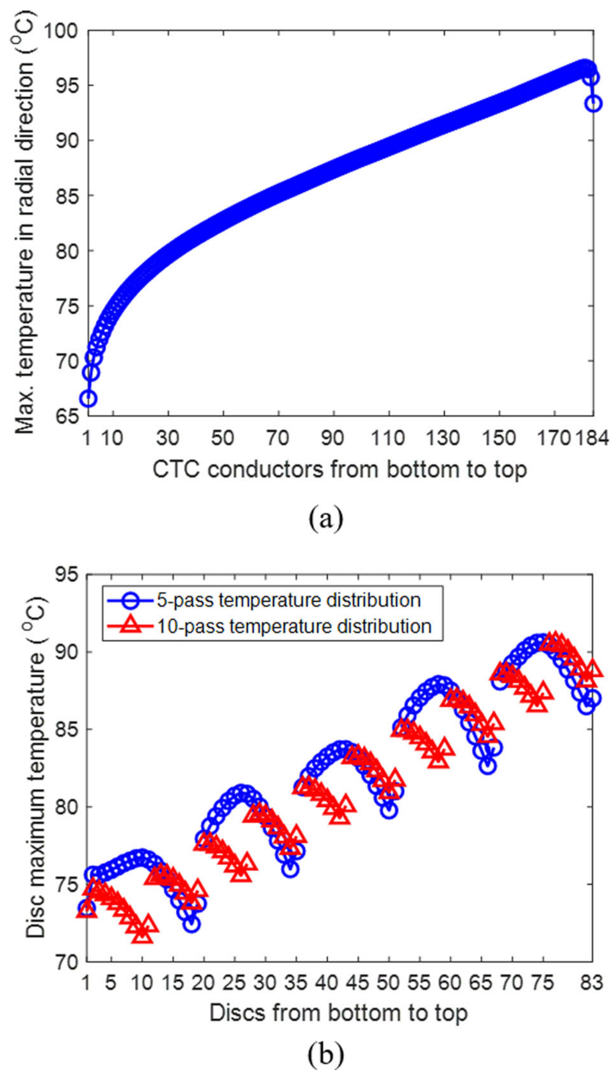

FIGURE 7 Temperature distributions in the OD cooling mode. (a) Maximum conductor temperatures in radial direction in the S disc-type winding. (b) Maximum disc temperature distributions in 5-pass and 10-pass disc-type windings

TABLE 3 Comparisons of pressure drop and temperatures for the OD cooling mode

	S disc-type IV 0.26 m/s	S disc-type IV 0.07 m/s	5-pass IV 0.07 m/s	10-pass IV 0.07 m/s
Δp (Pa)	616	137	623	1124
Top oil (°C)	63.6	78.4	78.4	78.4
Ave. wdg (°C)	76.4	86.8	80.0	78.8
Hotspot (°C)	81.8	97.2	91.2	91.2
h_{ave} (W/(K · m^2))	94	78	125	140

The pressure drops in conventional disc-type windings are roughly proportional to the number of passes. In addition, the ratio of conventional disc-type winding pressure drop to S disc-type winding pressure drop is also roughly the number of passes. When the total oil flow rate in the S disc-type winding is

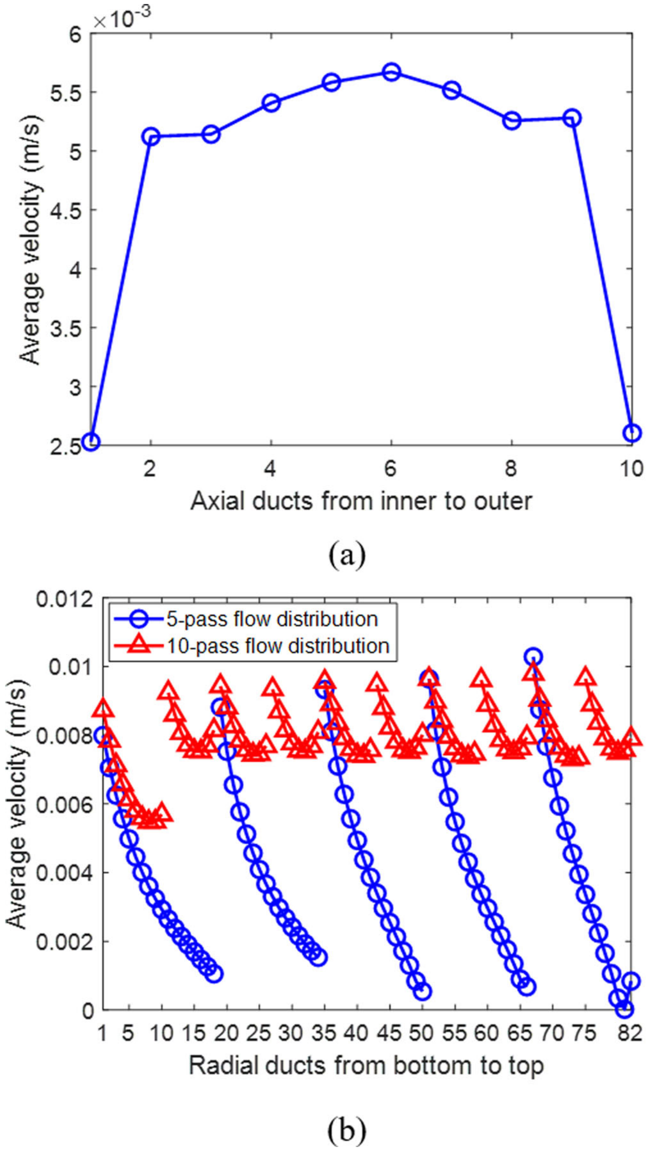

FIGURE 8 Flow distributions in the ON cooling mode with winding inlet velocity being 0.01 m/s. (a) Flow distribution in S disc-type winding axial ducts. (b) Flow distribution in 5-pass and 10-pass disc-type winding radial ducts

increased to match the pressure drop, the temperatures of top oil, average winding and hotspot are all significantly decreased, as shown by the case of winding inlet velocity being 0.26 m/s and pressure drop 616 Pa in Table 3. It is worth noting that the total oil flow rate in the winding for a given pump is determined by the pressure drop in the complete cooling loop, and therefore the proportion of the winding pressure drop to the total pressure drop in the loop determines the oil flow rate in the S disc-type winding, which is out of the scope of this study. The average heat transfer coefficients (h_{ave}) for the cases based on corresponding average winding heat flux, average winding temperature and average oil temperature are shown in Table 3. h_{ave} reflects overall convective heat transfer performance and increases with total flow rate and the number of passes for conventional disc-type windings. However, it is not representative of local heat transfer coefficients, especially the one at the hotspot.

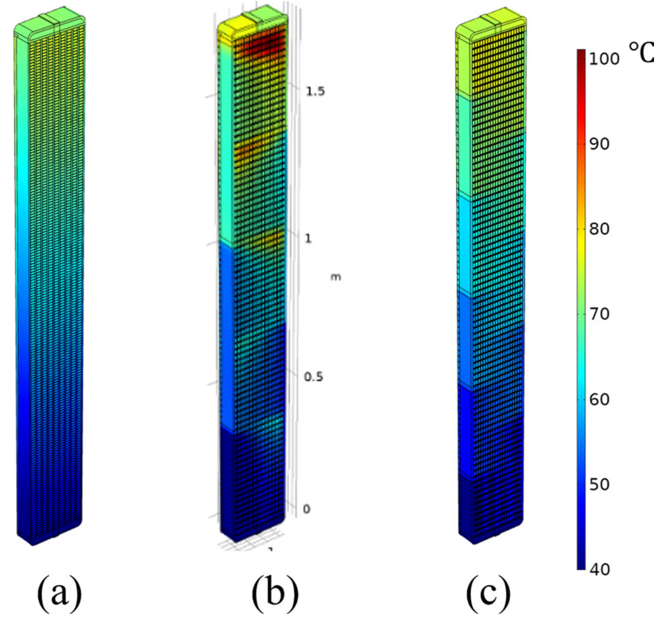

FIGURE 9 Temperature contours for the ON cooling mode. (a) S disc-type winding.
(b) 5-pass disc-type winding. (c) 10-pass disc-type winding

5.2 | ON cooling modes

For CFD comparisons in the ON cooling mode, the winding inlet velocity is 0.01 m/s. The oil flow distribution comparisons are shown in Figure 8. The axial flow distribution in the S disc-type winding is quasi-uniform, as shown in Figure 8a, similar to the OD scenario, and therefore results in quasi-uniform conductor temperature in the radial direction and almost linear conductor temperature distribution in the axial direction, as shown in Figures 9a and 10a respectively.

The flow distributions in the 5-pass and 10-pass conventional disc-type windings are uneven, and the flow distribution trend is opposite to that in the OD cooling mode. Higher flow rates are in the bottom part of the pass and lower flow rates in the top part of the pass. For the 5-pass winding, the oil flow rate in the penultimate radial duct of the top pass is reversed, as shown in Figure 8b, leading to an almost flow-stagnant region and significantly overheated region, as shown in Figures 9b and 10b. The drop of the top disc temperature of the 5-pass winding is because the top disc is adjacent to the downstream pass bottom radial duct that has a relatively high flow rate. The 10-pass winding temperatures are quasi-uniform in each pass as shown in Figures 9c and 10c due to relatively high and similar flow rates in the radial ducts as shown in Figure 8b.

The comparison of the pressure drop over the winding in Table 4 shows that the S disc-type winding has a much lower pressure drop than those of the 5-pass and 10-pass windings.

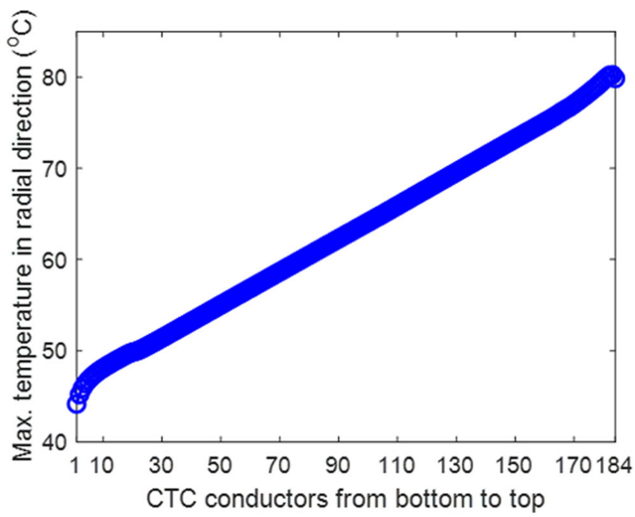

(a)

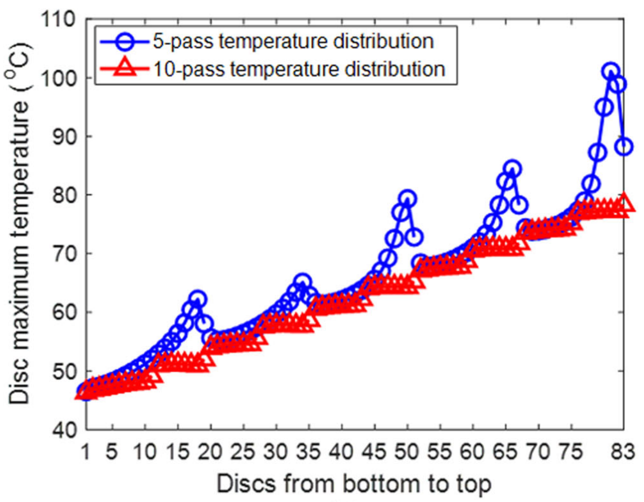

(b)

FIGURE 10 Temperature distributions in the ON cooling mode. (a) Maximum conductor temperatures in radial direction in the S disc-type winding. (b) Maximum disc temperature distributions in 5-pass and 10-pass disc-type windings

The pressure drop in the 5-pass and 10-pass windings are not proportional to the number of passes. The average winding temperatures are comparable among the windings. However, the hotspot temperature of the 5-pass winding is much higher than the other two, due to the occurrence of reverse flow. With the same total oil flow rate, the 10-pass winding has the lowest hotspot temperature at the expense of the highest pressure drop. However, it is worth noting that having more passes in conventional disc-type winding is not necessarily better because the resultant higher pressure drop brings lower total oil flow rate in the winding and can therefore lead to higher temperatures. Like OD cooling modes, the average heat transfer coefficient (h_{ave}) increases with the number of passes for conventional disc-type windings, but it is not representative of local heat transfer coefficients at the hotspot.

TABLE 4 Comparisons of pressure drop and temperatures for the ON cooling mode

	S disc-type IV 0.01 m/s	5-pass IV 0.01 m/s	10-pass IV 0.01 m/s
Pressure drop (Pa)	37	95	123
Top oil (°C)	74.1	74.1	74.1
Average winding (°C)	62.4	62.6	60.8
Hotspot (°C)	80.4	101.1	78.3
h_{ave} (W/(K · m^2))	66	64	94

6 | HEAT TRANSFER ENHANCEMENT FOR S DISC-TYPE WINDINGS

The S disc-type winding has robust thermal performance because of its quasi-uniform flow distribution in the axial cooling ducts, irrespective of the total oil flow rate or cooling modes. However, the top oil, average winding and hotspot temperatures in OD cooling modes can be close to the limits set in international standards for some flow rates as shown in Table 3. Therefore, there may be a need to further improve the OD thermal performance by enhancing the convective heat transfer in the long axial cooling ducts. The enhancement can be achieved by redeveloping the flow hydraulically and thermally in the axial ducts [19].

When the S disc-type winding is subjected to uniform power losses with winding inlet velocity being 0.16 m/s, the evolutions of winding and oil temperatures and the heat transfer coefficient in the axial duct are shown in Figure 11. It is worth noting that the oil temperature is set to rise linearly from bottom oil temperature to top oil temperature in the axial duct based on energy conservation, while the winding temperature, based on actual temperature extraction, rises with a decreasing slope, as shown in Figure 11a. The corresponding heat transfer coefficient decreases rapidly at the duct entrance region and then levels off as the flow gets further developed down the axial duct. The typical OD heat transfer coefficient ranges from 300 to 100 W/(K · m^2), as shown in Figure 11b. The rise of the heat transfer coefficient at the top end of the axial duct is caused by the presence of the radial cooling duct between the winding and the stress ring.

6.1 | Heat transfer enhancement by partitioning

To enhance the convective heat transfer, the efficient heat transfer in the entrance region can be exploited by inserting washers to make the flow redevelop, as shown in Figure 12. The washer inserted in this illustration is a thin layer of 1 mm thick. It replaces two winding discs and is placed in the middle of the two discs, creating two radial cooling ducts. A 20 mm wide opening is provided in the middle of the washer to guarantee quasi-uniform flow distribution in the downstream axial

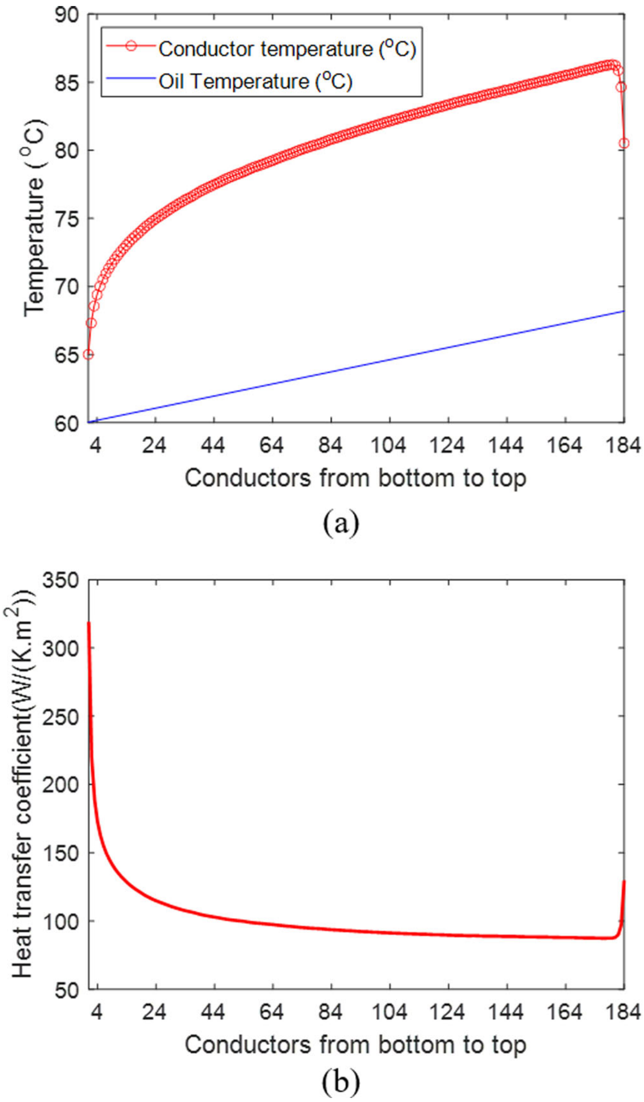

FIGURE 11 Variation of temperatures and heat transfer coefficient in the axial cooling duct. (a) Variations of winding and oil temperatures. (b) Variation of heat transfer coefficient in axial cooling ducts

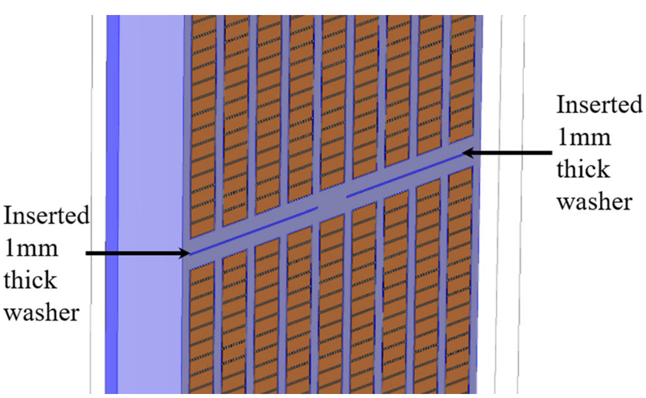

FIGURE 12 Insert of washers to partition the S disc-type winding

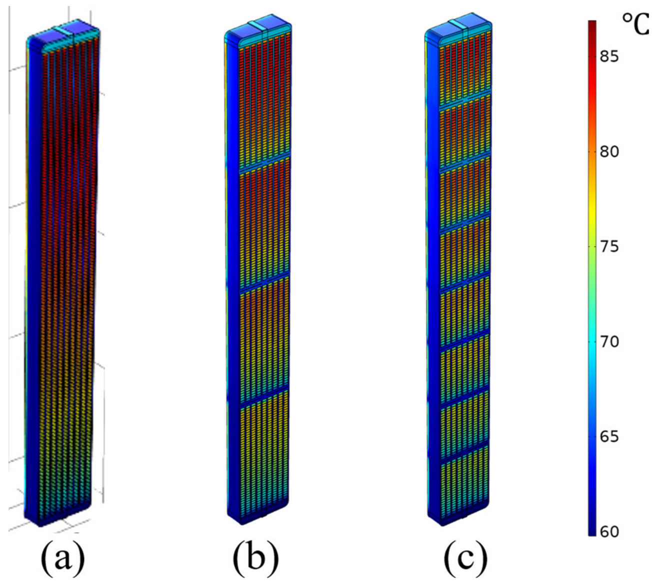

FIGURE 13 Temperature contours for partitioned S disc-type winding for the OD cooling mode with winding inlet velocity being 0.16 m/s. (a) 1-section (original) S disc-type winding. (b) 4-section S disc-type winding. (c) 8-section S disc-type winding

TABLE 5 Comparisons of temperatures and pressure drop for partitioned S disc-type windings with uniform power losses in the OD cooling mode with winding inlet velocity being 0.16 m/s

	Average winding (°C)	Hotspot (°C)	Pressure drop over the winding (Pa)
1-section	80.1	86.9	302
4-section	77.4 (−2.7)	85.5 (−1.4)	387
8-section	73.9 (−6.2)	84.3 (−2.6)	487

cooling ducts, as is the case for the winding top and bottom structure.

For the OD cooling mode with uniform power losses and winding inlet velocity being 0.16 m/s, the temperature contours of the original S disc-type winding and windings partitioned equally into four sections and eight sections are shown in Figure 13. It is worth noting that for the partitioned windings, the power losses are correspondingly increased to keep the same total power loss to the original S disc-type winding. It is obvious to see the enhancement of heat transfer at the bottom part of each section from the temperature contours in Figure 13 as well as the temperature distributions in the axial direction in Figure 14. The comparisons of temperatures in Table 5 show that the reduction of the average winding temperature is more pronounced than the reduction of the hotspot temperature. In addition, the pressure drop over the winding increases with the increase in the number of sections, but the pressure drop increase arising from partitioning the S disc-type winding is much lower than the case of increasing the number of passes in a conventional disc-type winding.

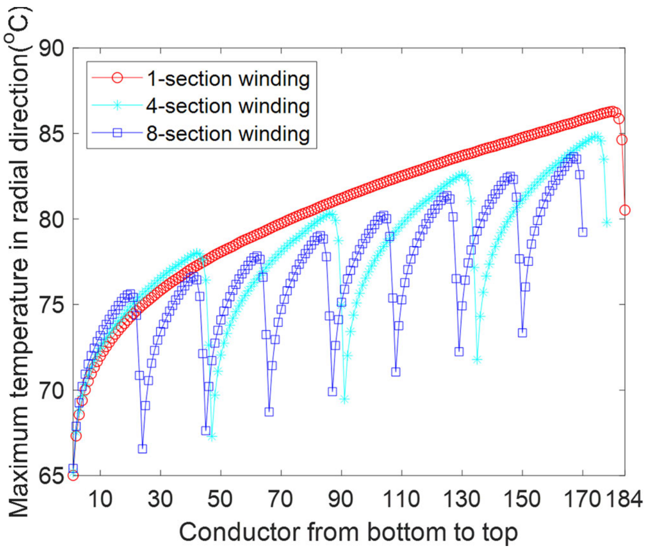

FIGURE 14 Variation of maximum conductor temperatures in radial direction for partitioned S disc-type windings

TABLE 6 Comparisons of temperatures and pressure drop for original and optimized S disc-type windings with uniform power losses

		Average winding (°C)	Hotspot (°C)	Pressure drop over the winding (Pa)
IV 0.16 m/s	1 section	80.1	86.9	302
	3 sections	75.1 (−5.0)	82.6 (−4.3)	384
IV 0.07 m/s	1 section	86.2	97.2	127
	3 sections	82.9 (−3.3)	93.4 (−3.8)	134

6.2 | Optimisation of partitioning

From a manufacturing perspective, the number of partitioning should be minimized to simplify the assembling and control the cost. A straightforward question follows on from this demand that is how to partition the winding into two sections and minimize the hotspot temperature. This will be investigated theoretically and then verified by CFD simulations in this section.

In the theoretical analysis, the winding is simplified into an axial cooling duct and it is assumed to be a 2D duct between 2 parallel plates. It is also assumed that once the duct is partitioned the flow redevelops with uniform velocity and temperature profiles. Based on the winding geometric dimensions, the average velocity in the axial duct is about 0.45 times the inlet velocity (IV) of the winding. The variation of heat transfer coefficient, h, along the axial duct is obtained through local Nusselt number (Nu). The relationship of local Nu and the dimensionless entrance length x^* is obtained by correlating results from thousands of planar 2D duct CFD simulations that took into account the effect of temperature dependent oil properties, as detailed in [20].

$$Nu = \begin{cases} 1.734x^{*-0.327} & x^* \leq 0.001 \\ 8.577 + 9.350(1000x^*)^{-0.518}e^{-141x^*} & x^* > 0.001 \end{cases} \tag{1}$$

The distance between the duct entrance and the partitioning location is x, and the total duct length is L. For this axial duct, the hotspot temperature is either at the top of the duct (T_L) or at the partitioning point (T_x). The hotspot temperature consists of four components: the inlet average oil temperature (T_{in}), the rise of the average oil temperature adjacent to the hotspot over the inlet oil temperature ($2 \cdot q'' \cdot S \cdot L/(\dot{m} \cdot c_p)$ or $2 \cdot q'' \cdot S \cdot x/(\dot{m} \cdot c_p)$, based on energy conservation and the factor 2 is included because of heat flux from both walls), the temperature gradient between the winding paper surface and the average oil (q''/h_x or q''/h_{L-x}, based on Newton's law of cooling), and the temperature gradient across the paper insulation ($q'' \cdot d_p/k_p$, based on Fourier's law of thermal conduction).

$$T_L = T_{in} + 2 \cdot q'' \cdot S \cdot L/(\dot{m} \cdot c_p) + q''/h_{\mathrm{L-x}} + \mathrm{q}'' \cdot d_p/\mathrm{k_p} \tag{2}$$

$$T_x = T_{in} + 2 \cdot q'' \cdot S \cdot x/(\dot{m} \cdot c_p) + q''/h_{\mathrm{x}} + \mathrm{q}'' \cdot d_p/\mathrm{k_p} \tag{3}$$

The predicted evolutions of T_L and T_x with the partitioning location, x, are shown in Figure 15 for winding inlet velocity of 0.16 and 0.07 m/s scenarios. The intersecting points indicate the optimal partitioning locations, which is 1.543 m for the case of inlet velocity being 0.07 m/s, and 1.336 m for inlet velocity being 0.16 m/s. With the decrease in winding inlet velocity, the optimal partitioning point shifts upwards. Further studies show that for ON inlet velocities, the optimal partitioning point is near the top of the winding, making the reduction of hotspot temperature less than 1 °C. It is worth noting that the temperatures in the ON cooling mode are much lower than the limits set in international standards, and therefore heat transfer enhancement is not a pressing need.

In practice, however, the two-section winding needs to be modified into a 3-section winding to keep the symmetry property of the winding geometry in the axial direction for a symmetric magnetic flux leakage distribution and therefore a balanced electromagnetic force in the axial direction to avoid axial shift of the winding [6]. The temperature contours of the 3-section windings are shown in Figure 16. Comparisons of temperatures and pressure drop in Table 6 show that the optimized partitioning leads to even more efficient hot-spot temperature reduction than the 8-section partitioning, and the resultant pressure drop increase is minimized. It is worth noting that the CFD simulations show higher hotspot temperature reduction than the predictions from Figure 15 based on Equations (2) and (3). This is because the first partitioning at the bottom of the winding further decreases the hotspot temperature. In addition, the flow distribution in the axial ducts features higher flow rates in the middle ducts and this flow distribution facilitates the cooling of the hot winding middle parts.

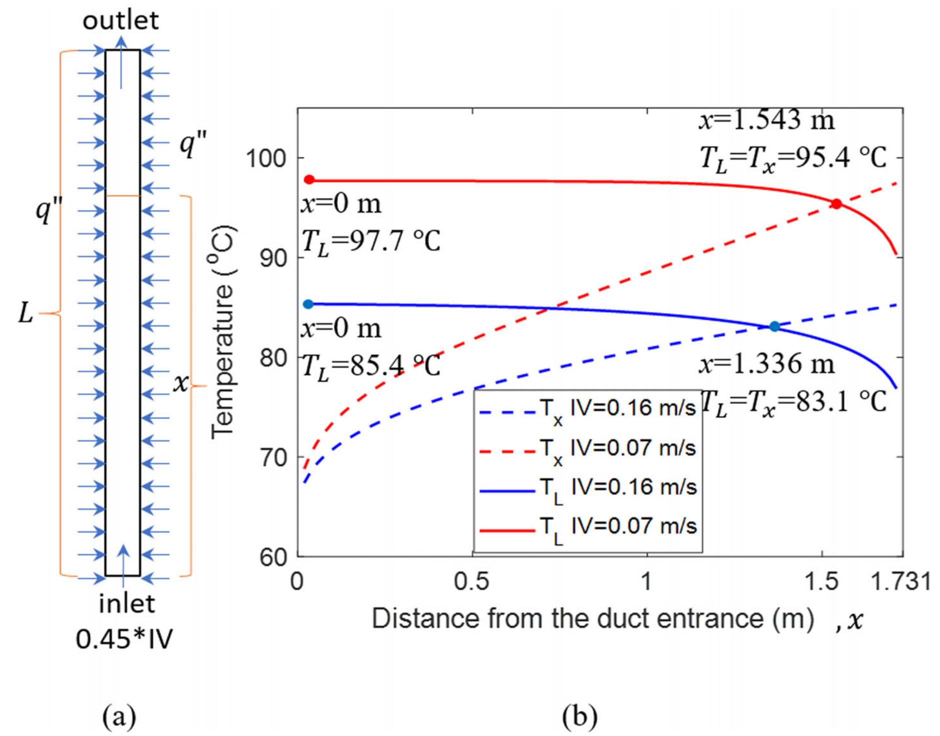

FIGURE 15 Optimisation of partitioning with inlet velocity (IV) being 0.16 m/s and 0.07 m/s. (a) Schematic illustration of partitioning into two sections. (b) Theoretical prediction of optimal partitioning location

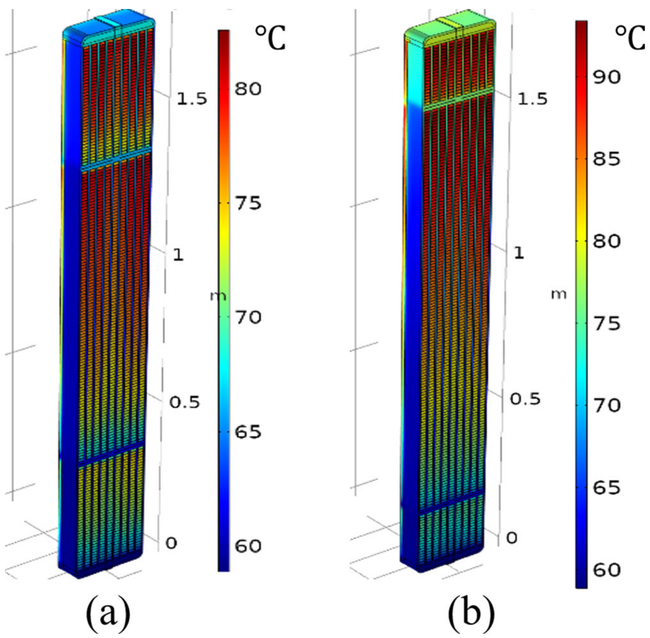

FIGURE 16 Temperature contours for optimized S disc-type winding partition in OD cooling modes. (a) Winding inlet velocity 0.16 m/s (b) Winding inlet velocity 0.07 m/s

7 | CONCLUSION

The thermal behaviour of the S disc-type winding which has only axial cooling ducts and physically resembles a layer-type winding, has been investigated and compared with that of converted conventional disc-type windings in steady state conditions. The flow and temperature distribution results for the two types of windings are representative for other dimensions. The following more detailed conclusions can be drawn from this study:

1. Owing to the openings in the middle of the stress rings, the S disc-type winding has quasi-uniform oil flow distribution in the axial cooling ducts, irrespective of the winding total oil flow rate or the cooling modes. The quasi-uniform flow distribution results in robust thermal performances in terms of consistency and gradual change of the hotspot temperature with the total oil flow rate.
2. Conventional disc-type windings experience much higher pressure drop over the winding than the S disc-type winding and the flow distribution in the radial cooling ducts can be severely uneven and therefore result in localized overheating for both OD and ON cooling modes. Control of flow distribution is critical for conventional disc-type winding thermal design.
3. The thermal performance of the S disc-type winding in OD cooling modes can be further enhanced by axially partitioning the winding into multiple sections and making the flow redevelop hydraulically and thermally. The partitioning can be optimized to achieve more hotspot temperature reduction (of about 4 °C) with a smaller pressure drop increase (approximately 10–30%). On the other hand, the thermal effects of partitioning for ON cooling modes are negligible.

ACKNOWLEDGEMENTS

The authors would like to express their gratitude to EPRI, M&I Materials, National Grid, Scottish Power, SGB-SMIT, Shell, TJ|H2b and Weidmann for their financial and technical contributions to the Transformer Research Consortium.

CONFLICT OF INTEREST

The authors declare no conflict of interest.

NOMENCLATURE

A	Cross sectional area of the cooling duct (m^2)
C_p	Oil specific heat ($J/(kg \cdot K)$)
D_h	Hydraulic diameter ($D_h = 4 \cdot A/p$) (m)
d_p	Paper thickness (m)
h	Heat transfer coefficient ($W/(K \cdot m^2)$)
h_{L-x}	Heat transfer coefficient at the top of the duct with entrance length being L-x ($W/(K \cdot m^2)$)
h_x	Heat transfer coefficient at the partitioning location with entrance length being x ($W/(K \cdot m^2)$)
IV	Average inlet velocity for the winding (m/s)
k	Oil thermal conductivity ($W/(K \cdot m)$)
k_p	Paper thermal conductivity ($W/(K \cdot m)$)
$\dot{m}$	Mass flow rate in the duct (kg/s)
Nu	Nusselt number ($Nu = h \cdot D_h/k$)
p	Perimeter of the cooling duct (m)
Pr	Prandtl number ($Pr = \mu \cdot c_p/k$)
q''	Heat flux on the surface of the winding (W/m^2)
Re	Reynolds number ($Re = \rho \cdot u_m \cdot D_h/\mu$)
S	Winding surface area on one side of the duct (m^2)
T_{in}	Oil temperature at the inlet of the duct (°C)
T_L	Oil temperature at the top of the duct (°C)
T_x	Oil temperature at the partitioning location (°C)
u_m	Oil average velocity in the cooling duct (m/s)
x	Distance from the duct entrance (m)
x^*	Dimensionless entrance length ($x^* = x/(Re \cdot Pr \cdot D_h)$)
μ	Oil dynamic viscosity ($Pa \cdot s$)
ρ	Oil density (kg/m^3)

ORCID

Zhongdong Wang https://orcid.org/0000-0002-6006-9566

REFERENCES

1. IEC Standard 60076–7: Loading guide for oil-immersed power transformers (2018)
2. IEEE C57.91: Guide for loading mineral-oil-immersed transformers and step-voltage regulators (2011)
3. IEC Standard 60076-2: Temperature rise for liquid-immersed transformers (2011)
4. Koch, M., Tenbohlen, S.: Evolution of bubbles in oil–paper insulation influenced by material quality and ageing. IET Electr. Power Appl. 5(1), 168–174 (2011).
5. Hill, J., Wang, Z.D., Liu, Q., Krause, C., Wilson, G.: Analysing the power transformer temperature limitation for avoidance of bubble formation. High Voltage 4(3), 210–216 (2019).
6. Heathcote, M.: J&P Transformer Book, Thirteenth ed., Newnes, New South Wales, Australia (2007)
7. CIGRE659: Transformer Thermal Modelling. Technical Brochure, (2016)
8. Zhang, X., Wang, Z.D., Liu, Q.: Prediction of pressure drop and flow distribution in disc type transformer windings in an od cooling mode. IEEE Trans. Power Delivery 32(4), 1655–1664 (2017).
9. Tenbohlen, S., Schmidt, N., Breuer, C., Khandan, S., Lebreton, R.: Investigation of thermal behavior of an oil-directed cooled transformer winding. IEEE Trans. Power Delivery 33(3), 1091–1098 (2018).
10. Daghrah, M., Zhang, X., Wang, Z.D., Liu, Q., Jarman, P., Walker, D.: Flow and temperature distributions in a disc type winding-part I: Forced and directed cooling modes. Appl. Therm. Eng. 165, 114653 (2020).
11. Skillen, A., Revell, A., Iacovides, H., Wu, W.: Numerical prediction of local hot-spot phenomena in transformer windings. Appl. Therm. Eng. 36, 96–105 (2012).
12. Torriano, F., Picher, P., Chaaban, M.: Numerical investigation of 3d flow and thermal effects in a disc-type transformer winding. Appl. Therm. Eng. 40, 121–131 (2012).
13. Zhang, X., Wang, Z.D., Liu, Q., Negro, M., Gyore, A., Smith, P.W.R.: Numerical investigation of influences of liquid types on flow distribution and temperature distribution in disc type on cooled transformers. In: The 19th IEEE International Conference on Dielectric Liquids (ICDL), Manchester, UK (2017)
14. Zhang, X., Daghrah, M., Wang, Z.D., Liu, Q.: Flow and temperature distributions in a disc type winding-part II: Natural cooling modes. Appl. Therm. Eng. 165, 114616 (2020).
15. Zhang, X., Wang, Z.D., Liu, Q., Jarman, P., Negro, M.: Numerical investigation of oil flow and temperature distributions for on transformer windings. Appl. Therm. Eng. 130, 1–9 (2018).
16. Torriano, F., Campelo, H., Quintela, M., Labbé, P., Picher, P.: Numerical and experimental thermofluid investigation of different disc-type power transformer winding arrangements. Int. J. Heat Fluid Flow 69, 62–72 (2018).
17. Hulsink, G.J.: Method of Making a Transformer Winding in the Form of a Disc Winding Provided with Axial Channels. U.S. Patents 5,167,063, 1 Dec. 1992
18. Zhang, X., Daghrah, M., Wang, Z.D., Liu, Q., Jarman, P., Negro, M.: Experimental verification of dimensional analysis results on flow distribution and pressure drop for disc type windings in od cooling modes. IEEE Trans. Power Delivery 33(4), 1647–1656 (2018).
19. Bergman, T.L., Incropera, F.P., DeWitt, D.P., Lavine, A.S., Fundamentals of Heat and Mass Transfer, John Wiley & Sons, Hoboken, NJ (2011)
20. Zhang, X., Wang, Z.D., Liu, Q., Jarman, P., Gyore, A., Dyer, P.: Investigation of convective heat transfer efficiency in the horizontal cooling duct of a disc type transformer winding. In: *The 19th International Symposium on High Voltage Engineering (ISH)*, Pilsen, Czech Republic (2015)

How to cite this article: Zhang, X., Liu, Q., Wang, Z., Wilkinson, M.: Comparisons of transformer thermal behaviours between conventional disc type and S disc type windings. IET Gener. Transm. Distrib. 16, 703–714 (2022). https://doi.org/10.1049/gtd2.12321